NORTHWESTERN
UNIVERSITY

Center for Science and Protection of Engineered Environments (SPREE)

Department of Civil and Environmental Engineering

McCormick School of Engineering and Applied Science

Evanston, Illinois 60208, USA

Small-scale Geotechnical Testing Using a Six-axis Robot

Z. Jin, Z. Shi, J.P. Hambleton

SPREE INTERNAL REPORT No. 20-7/495S

July 2020

Small-scale Geotechnical Testing Using a Six-axis Robot

Zhefei Jin[a], Zhenhao Shi[b], James Hambleton[a]

[a]*Department of Civil and Environmental Engineering, Northwestern University, Evanston, IL 60208, U.S.A*

[b]*Department of Geotechnical Engineering, Tongji University, Shanghai, 200092, China*

Abstract

Single-gravity (1-g) small-scale testing is a widely used method to investigate geomechanics problems that involve the interactions between soils and objects (e.g., structures or machine parts). This letter presents a new approach for performing 1-g model tests where a six-axis industrial robot functions as a versatile actuator capable of moving objects along virtually arbitrary trajectories, while simultaneously tracking multiple components of force and moment acting on the objects. A performance evaluation confirms that the robot's motion control and force measurement are sufficiently accurate for geotechnical model tests. This assessment is completed through two benchmarking exercises: (1) determining the failure envelope of a strip foundation subjected to combined loading and (2) quantifying the force-displacement history for the soil cutting process (e.g., for applications in soil-machine interaction).

Keywords: laboratory testing; physical modeling; robot; actuation; soil-machine interaction

1. Introduction

Geomechanics problems, particularly those involving the interactions between soils and objects (e.g., structures or machine parts), can be experimentally investigated at full scale (Negro et al., 2000; Jude et al., 2002; Todorovska, 2002; Antille et al., 2013) or smaller scales more amenable to laboratory testing (Gottardi and Butterfield, 1993; Araya et al., 1996; Dou and Byrne, 1996; Calvetti et al., 2004; Nezami et al., 2007; Vahed

Email addresses: ZhefeiJin2015@u.northwestern.edu (Zhefei Jin), 19613@tongji.edu.cn (Zhenhao Shi), jphambleton@northwestern.edu (James Hambleton)

et al., 2008; Moreland et al., 2011; Nasr, 2013). In some cases, especially for problems in soil-machine interaction, characteristic lengths are sufficiently small that full-scale testing can be completed in the laboratory without concern for scaling issues. As compared to field testing, physical modeling in the laboratory has the advantage that loading conditions, drainage conditions, soil stratigraphy, and other test details can be well controlled. Single-gravity small-scale testing represents a simple and economical way to explore the phenomenological behavior without being constrained to conditions on a specific site, and when used as a substitute for full-scale testing, the errors produced by the lower soil stress levels can often be corrected by adjusting soil properties, structure geometry, and loading rate (Byrne and Houlsby, 2004; Leblanc et al., 2010; Abadie et al., 2018; Robinson et al., 2019) or by using correction factors determined through dimensional analysis and scaling (Hettler, 2010; Lauder and Brown, 2014; Slonaker et al., 2017). Additionally, 1-g tests often permit the use of larger soil samples, which can reduce sample disturbance due to the installation of instruments and mitigate errors associated with the size of the soil particles relative to object dimensions (Wood, 2014).

The sophistication of testing apparatus, particularly with regard to the actuating system, depends on the complexity of the mechanical process one intends to model. Advanced actuating systems capable of generating motion and force in multiple directions are needed for problems routinely encountered in geotechnical engineering (e.g., foundation subjected to combined loading). Examples of problems that lie at interfaces with other disciplines include soil excavation (Maciejewski and Jarzebowski, 2002), soil-wheel interaction for off-road vehicle mobility (Wong and Reece, 1967; Wu et al., 1984; Khot et al., 2007; Ding et al., 2011), and the locomotion of legged and wheeled robots on earth and other planets (Bauer et al., 2005; Li et al., 2013; Lynch et al., 2020). Physical modeling completed to date has largely rested on the use of customized multi-degree-of-freedom actuation systems (Ding et al., 2011; Qian and Goldman, 2015; O'Loughlin et al., 2018). While the robotic arms used ubiquitously in manufacturing have tremendous potential for use as multi-degree-of-freedom actuators, and indeed some existing studies have made use of these (Goldman, 2014; Hong, 2001; Li et al., 2012, 2013), standard industrial robots

have yet to be validated and accepted as actuators for physical modeling.

The aim of this paper is to demonstrate the utility and validity of using a standard industrial robot as an actuating system for 1-g small-scale geotechnical tests. This approach offers four remarkable benefits. First, the robot can move objects along a virtually arbitrary trajectory with industrial-grade precision. This feature, augmented by an integrated force sensor capable of simultaneously measuring multiple components of force and moment, makes the robot an ideal platform for modeling various types of interaction problems. Second, the robot is fully programmable in that all operations can be prescribed, executed automatically, and readily repeated. Third, industrial robots are manufactured by standardized processes that are typically subject to rigorous quality control, and thus their performance is reliable and predictable. Lastly, and perhaps most importantly, industrial robots are now widely available at costs that continue to decrease, in much the same way that personal computers have proliferated and economized with advances in hardware and software. Once industrial robots are fully validated as being suitable for geotechnical model testing, the same approach can be rapidly adopted in laboratories across the world. This work begins to provide such validation.

In the following sections, we first evaluate performance of the selected robot with respect to controlling motion and accurately measuring components of force and moment. Then, results for two benchmark tests are presented to demonstrate the application of the robot to a conventional problem in geotechnical engineering and a problem in the emerging area of soil-machine interaction.

2. Robot performance evaluation

Figure 1(a) shows the general arrangement of the laboratory in which all tests for this study were completed. The robot is an IRB-4400 six-axis robot manufactured by ABB and mounted to the reinforced concrete floor of the laboratory with a $813 \times 711 \times 32\,\text{mm}$ steel base plate as per manufacturer specifications. The six axes and their corresponding motions are depicted in Figure 1(b). For detailed discussions on the kinematics of such articulated robot, we refer the reader to literature on modern robotics (e.g., Koren, 1985;

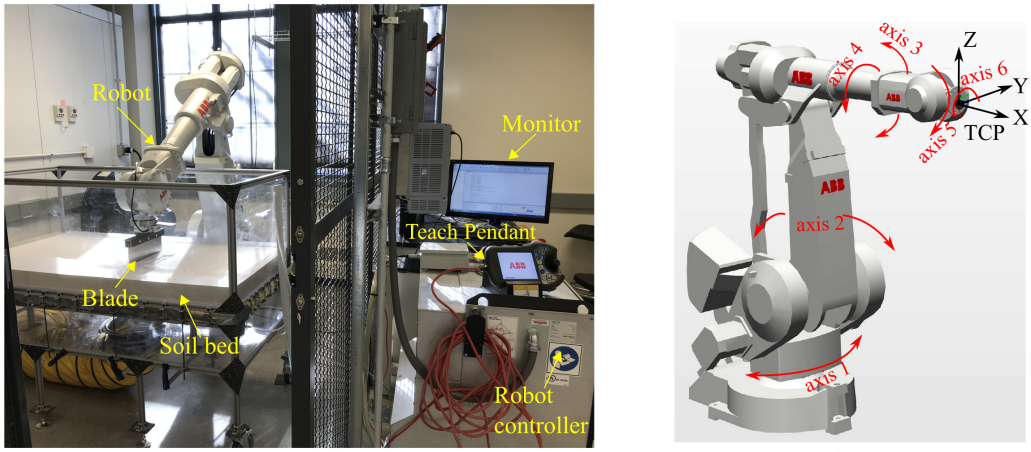

(a) (b)

Figure 1: Robot-based testing facility. Subfigure (a) shows the main components, including the six-axis industrial robot, its control system, a soil bed, and an object that interacts with the soil. Subfigure (b) shows the Cartesian coordinate system associated with the tool center point (TCP) and the six independent joints that control the motion of the TCP: axis 1 allows the rotation of the entire robot against its base (through a horizontal plane); axis 2 controls the forward and backward extension of the lower arm; axis 3 extends the vertical reach by raising and lowering the upper arm; axis 4, also known as wrist roll, rotates the upper arm along its longitudinal axis; axis 5 rotates the wrist of the robotic arm; axis 6 is responsible for the twisting of the wrist (i.e., circular motion around the X-axis as depicted).

Murray, 2017). Any object used to model structures or machines (e.g., the blade shown in Figure 1(a)) is attached to the tip of the robotic arm, hereafter referred to as the tool center point (TCP), shown in Figure 1(b). Accordingly, interaction processes between objects and soils can be modeled by either explicitly prescribing the trajectories of the TCP (i.e., displacement control) or implicitly controlling TCP position by specifying forces or moments (i.e., force control). This letter focuses only on displacement control.

The robot uses rotary encoders associated with the six axes to track the position of the TCP. This recording of position is hereafter referred to as 'internal position.' There can be a difference between the internal position and the actual TCP position due to various factors, including the robot's precision, compliance of the robot, and mounting tolerances. To quantify the difference between internal and actual position, we measured TCP position independently using a linear potentiometer displacement transducer (LPDT) manufactured by GDS Instruments. The LPDT was attached to the robot arm to connect the TCP and a fixed horizontal or vertical plane (e.g., floor or wall). By jogging the TCP towards the plane along its normal, the TCP displacement was simultaneously measured by the LPDT and the robot's internal system. The evaluation was repeated in 10 positions within the robot's working range to consider the influence of the spatial configuration of the robot arms on the measurement error. At each position, a force of 200 N acting in the direction of motion was applied to the TCP using a pulley and dead weights to replicate a typical external force expected during testing. Among all cases considered, application of the 200 N force while the robot was inactive produced a displacement of at most 0.35 mm, as measured using the LPDT (but not registered as a change in the internal position). This number reflects the total elastic stiffness of the robot arm and floor mount while the robot is inactive. While active, the displacements measured by the LPDT and the robot's recording of internal position differed by less than 0.25% (i.e., displacements less than 0.088 mm over the 35 mm range of the LPDT).

A six-axis load cell (Sunrise Instruments, #3314C) was supplied and installed at the tip of the robotic arm by the manufacturer. This load cell measures forces along three mutually perpendicular axes and three torques about the same axes. The accuracy of this

sensor was assessed by applying a known dead weight to the tip of a rigid bar connected to the load cell and then rotating along axis 6 (see Figure 1(b)) to align the force and moment generated by the dead weight with the load cell's different axes. For force and moment up to 200 N and 20 N·m (both reflect the expected maximum force and moment in normal tests), the relative measurement error was found to be less than 4%.

3. Benchmark tests

The two benchmark problems considered in this paper were selected for their different requirements on the experimental setup and for their differing relevance, with one pertinent to foundation engineering and the other relevant to soil-machine interaction. The first problem (strip footing under combined loading) involves relatively small displacements but rests crucially on the consideration of multiple loading components. The second (soil cutting test) requires actuation over a large range of displacements. The intention of presenting the examples is not to provide additional insight into the problems themselves but to demonstrate viability of using an industrial robot for actuation and accurate resolution of relevant forces and displacements.

All tests were performed using silica sand supplied by the U.S. Silica Company. The particles of this sand are round in shape and range in size from 0.075 mm to 0.425 mm, with a mean diameter of $D_{50} = 0.13$ mm. The coefficient of uniformity for the particles is $C_u = 1.65$, and the coefficient of curvature is $C_c = 1.13$. Hence, the sand is classified as poorly-graded (SP). The maximum density of this sand is $\rho_{max} = 1.73\,\mathrm{g/cm^3}$ (ASTM:D4253-16, 2016), and its minimum density is $\rho_{min} = 1.46\,\mathrm{g/cm^3}$ (ASTM:D4254-16, 2016). The peak friction angle of the sand was measured using direct shear tests. For specimens with a dry density of $1.70\,\mathrm{g/cm^3}$ (i.e., a relative density of $D_r = 90\%$), the peak friction angle was found to range from 47.6° to 32.7° over normal stresses ranging respectively from 20 kPa to 110 kPa. These measurements are reasonably close to the data presented by Lehane and Liu (2013) for so-called UWA sand, which is similar to the silica sand utilized in the present study (e.g., $D_{50} = 0.15$ mm for UWA sand). For a relative density of 80%, peak friction angles for UWA sand assessed using direct shear tests ranged from 43.5° to 38.5°

Figure 2: Experimental setup and procedures for evaluating the failure envelope of a strip footing under combined loads. (a) The dimensions of the model foundation, $L = 160\,\text{mm}$ and $B = 20\,\text{mm}$ (aspect ratio $L/B = 8$), ensure that the deformation can be approximated assuming plane strain, and the fixed connection to the robot eliminates rotation of the model foundation relative to the robot. (b) Straight-line trajectories are specified through the angle θ, with other symbols and sign conventions as depicted.

for normal stress ranging respectively from 20 kPa to 100 kPa.

3.1. Strip footing under combined loading

The behavior of a strip foundation under general planar loading has been thoroughly studied by small-scale testing (Vesic, 1963, 1975; Hansen, 1970; Gottardi and Butterfield, 1993; Georgiadis, 2010). To achieve different load combinations, these previous studies relied on sophisticated and highly customized apparatus involving loading frames, hydraulic jacks, motors, and other equipment in addition to the systems required to measure force and displacement. In this study, the model foundation is simply connected to the robot as shown in Figure 2(a) and then displaced into the soil along various trajectories (see Figure 2(b)) to achieve the desired loading path. In this study, only straight-line motion was assumed for simplicity, and the direction of motion is specified by the angle θ shown in Figure 2(b). The rate of the movement along each trajectory was kept at 0.02 mm/s to eliminate inertia effects. The tests were performed on sand beds prepared by the pluviation method described by Maillot (2013) to achieve a density of $D_r = 90\%$.

Figures 3(a)-(b) show the evolution of the vertical (V) and horizontal (H) forces (positive when acting as drawn in Figure 2(b)) for different trajectories obtained by

varying angle θ. In all cases, the measured moments were negligible, and they are thus not reported. The force-displacement curves are characterized by post-peak softening, typical of sands with low confinement and high relative density (Vesic, 1963, 1975; Kimura et al., 1985). The softening observed for horizontal force H further develops to a reversal of direction (i.e., sign change) for relatively steep trajectories ($\theta = 90°$, $76°$ and $63°$). While perhaps counterintuitive, these negative values can be explained by the nature of the failure mode for penetration-dominant motions, where motion of soil at the base of the foundation reverses the direction of relative sliding (i.e., the mass of soil below the foundation displaces leftward in Figure 2(b) with velocity larger than du_x/dt).

The failure of the footing along various trajectories can be encapsulated by an envelope characterizing the combination of forces and moments leading to the failure (Butterfield and Ticof, 1979; Ricceri and Simonini, 1989; Loukidis et al., 2008; Georgiadis, 2010). In Figure 3(c), the load paths corresponding to the different trajectories are plotted together with the failure envelope obtained by fitting a surface that bounds all load paths. The parabolic envelope proposed by Gottardi and Butterfield (1993), which has been extensively verified in the literature (e.g., Houlsby and Cassidy, 2002; Cassidy et al., 2002; Bienen et al., 2006; Govoni et al., 2010), is adopted here:

$$H = \beta_1 V[1 - (V/V_{max})^{\beta_2}] \tag{1}$$

where V_{max} is the bearing capacity under vertical load; $\beta_1 = \tan(\delta)$; δ is the friction angle of the footing-sand interface; β_2 is a fitting parameter. Figure 3(c) shows that the data can be well fitted by the analytical envelope, showing that the test results are consistent with established knowledge. From the fitting parameter $\beta_1 = 0.578$, one can infer a soil-foundation interface friction angle of $\delta = 30°$. When combined with the measured V_{max} and the bearing capacity solution given by Martin (2005), this implies a friction angle of $46°$ for the sands. This back-calculated property compares favorably with the friction angle of $47.6°$ measured from direct shear tests for a normal stress of 20 kPa (the lowest considered).

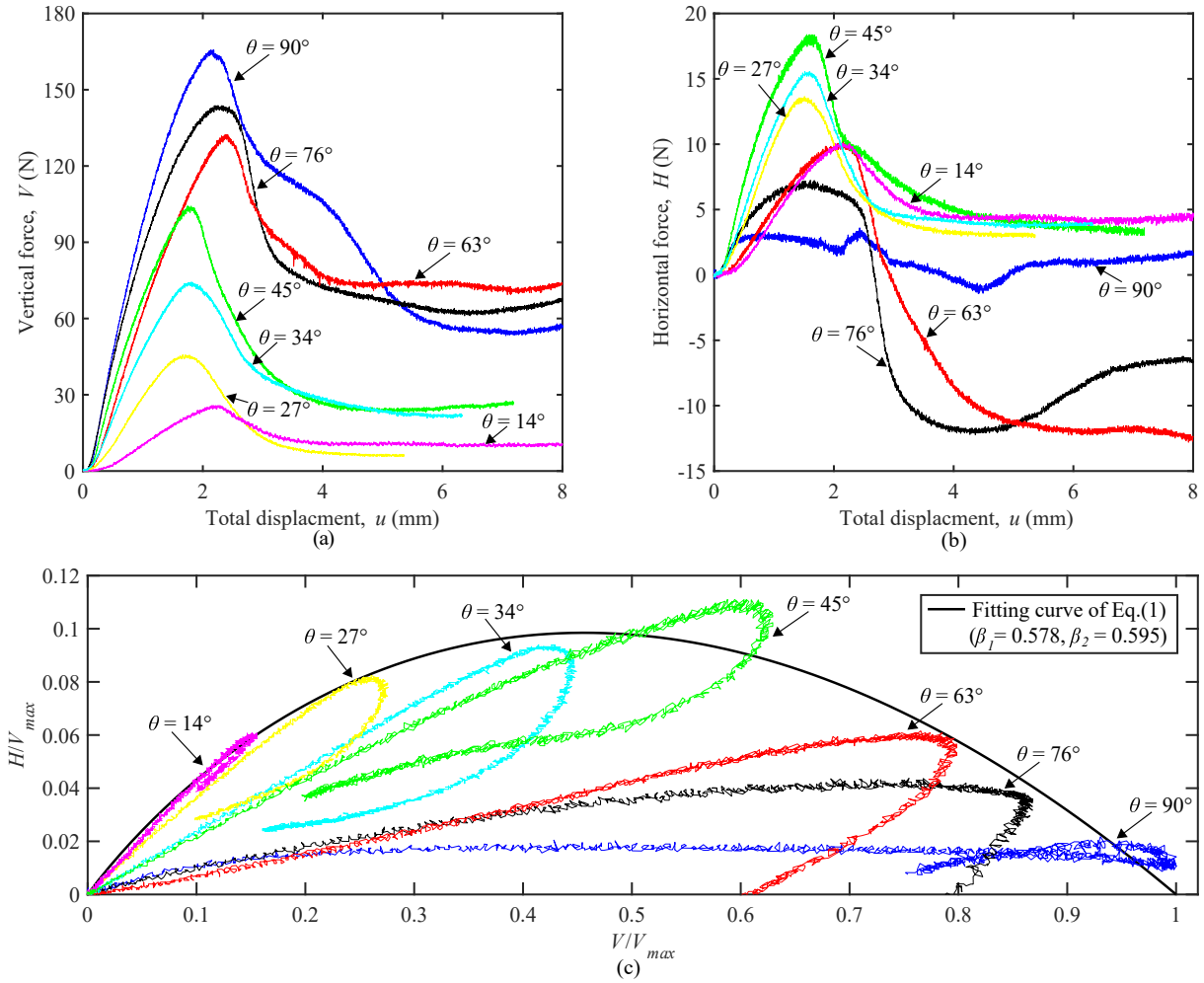

Figure 3: (a) Vertical and (b) horizontal force-displacement curves corresponding to the trajectories specified by θ (see Figure 2(b) for variable definitions), and (c) failure envelope for the strip foundation. Quantities are normalized by V_{max}, the maximum force attained under vertical load ($\theta = 90°$).

3.2. Soil cutting test

Soil cutting is a fundamental process in soil-machine interaction relevant to excavation and propulsion (Muro, 1989; Ding et al., 2011; Wong, 2012; Li et al., 2013; Wong, 2014; Askari and Kamrin, 2016). The cutting process is characterized by horizontal displacements that are many times larger than the embedment of the object, resulting in very large soil deformation (Selig and Nelson, 1964; Yong and Hanna, 1977; Hambleton et al., 2014; Kashizadeh et al., 2014; Gravish et al., 2010, 2014; Kobayakawa et al., 2018, 2019). In previous studies, tests were typically conducted using two linear actuators allowing for independent control of vertical and horizontal displacements (Hambleton et al., 2014; Kashizadeh et al., 2014; Gravish et al., 2010, 2014).

Figure 4(a) illustrates the setup for the soil cutting test completed using the six-axis robot. For these tests, samples were prepared using silica sand and fluidization method described by Jin et al. (2019) based on the studies of Goldman and co-workers (Qian and Goldman, 2015; Qian et al., 2015; Li et al., 2009, 2012, 2013; Maladen et al., 2009). The measured force-displacement relationship is given in Figure 4(b), which shows that sand density has a profound influence on the cutting responses. For dense sands, the cutting force features periodic jumps followed by gradual build-up of resistance. This peculiar response, which is attributed to successive shear band formations (Hambleton et al., 2014; Kashizadeh et al., 2014), is not observed for loose sand. The general trend of monotonically increasing resistance for cutting in loose sands represents a lower bound for the above-mentioned periodic drops, suggesting a convergence in the mode of deformation corresponding to critical state. These distinct behaviors for cutting in loose and dense sands are consistent with observations from previous studies (Gravish et al., 2010, 2014). The inset in Figure 4(b) shows high-frequency oscillations observed in the history of cutting force, which may result from the sudden movement of a single particle or the rearrangement of a few sand particles in a local neighborhood (Murphy et al., 2019).

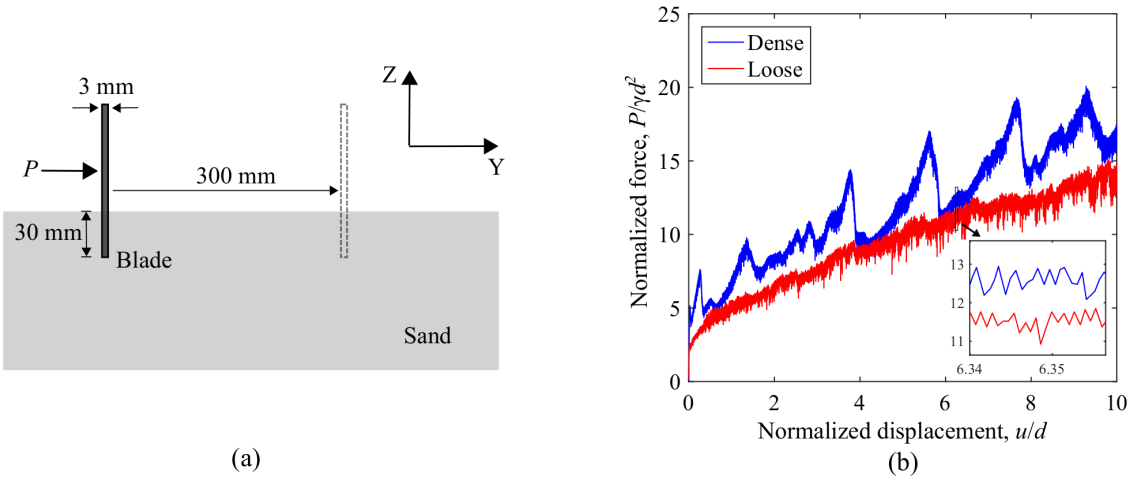

Figure 4: Soil cutting test setup, procedures, and results: (a) a thin blade with width of 3 mm and length of 300 mm is first penetrated into the sand to a depth of 30 mm, followed by lateral movement at a rate of 0.2 mm/s; (b) measured force-displacement history for cutting in the dense and loose sands characterized by $D_r = 90\%$ and $D_r = 18\%$, respectively. Data are presented in terms of dimensionless variables, where P is the lateral force on the blade, γ is the sand's unit weight, $d = 30$ mm is the penetration depth, and u is the horizontal displacement of the blade.

4. Conclusions

This paper presents the concept of using an industrial robot as an actuator for small-scale geotechnical testing. The selected six-axis robot can move attached objects along virtually any trajectory, and it is capable of operating over a large working range as needed for applications in soil-machine interaction. When combined with a six-axis load cell, this approach represents a unified platform for physical modeling of a wide variety of interaction processes between soils and structures (or machine parts). The increasing availability and decreasing cost of industrial robots suggest that such systems may become commonplace in laboratories around the world.

This study shows that the selected robot (an IRB-4400 six-axis robot manufactured by ABB) is capable of tracking objects' movements and measuring forces with the accuracy required by typical small-scale tests. Two benchmark tests demonstrate the applicability of the robot for studying conventional geotechnical problems and more complex interaction problems. These examples emphasize the ease of conducting tests with a commercially available robot, especially for problems involving multi-axial motions and responses that would otherwise require customized actuation, control, and measurement systems.

Industrial robots can also be used to complete tests under force control and to perform repetitive tasks automatically, two features that are not discussed in detail in this letter. The former feature expands the application of the robot to more complex problems where certain components of an object's motion must be implicitly controlled by fulfilling requirements on the corresponding force and/or moment components. The latter feature unlocks the possibility of achieving automated testing, where the robot-based actuator can be seamlessly integrated with other programmable components (e.g., automated specimen preparations (Maladen et al., 2009; Li et al., 2009; Qian et al., 2015) and visualization (Stanier and White, 2013; White et al., 2003)). The robot's automated functionality allows for more efficient completion of parametric studies, particularly for problems where a large number of trajectories must be explored (such as a footing subjected to combined loading). These aspects will be more thoroughly investigated in future work.

Acknowledgements

This material is based upon work supported by the National Science Foundation under Grant No. 1846817.

References

Abadie, C. N., Byrne, B. W. and Houlsby, G. T. (2018). Rigid pile response to cyclic lateral loading: laboratory tests, *Géotechnique* **69**(10): 863–876.

ABB Robotics. (2017). *Product Specification IRB 4400*, Retrieved from https://new.abb.com/products/robotics/industrial-robots/irb-4400.

Antille, D. L., Ansorge, D., Dresser, M. L. and Godwin, R. J. (2013). Soil displacement and soil bulk density changes as affected by tire size, *Transactions of the ASABE* **56**(5): 1683–1693.

Araya, K., Kudoh, M., Zhao, D., Liu, F. and Jia, H. (1996). Improvement of planosol solum: Part 1, experimental equipment, methods and preliminary soil bin experiments with ploughs, *Journal of Agricultural Engineering Research* **63**(3): 251–259.

Askari, H. and Kamrin, K. (2016). Intrusion rheology in grains and other flowable materials, *Nature Materials* **15**(12): 1274.

ASTM:D4253-16 (2016). Standard Test Methods for Maximum Index Density and Unit Weight of Soils Using a Vibratory Table, *ASTM International, West Conshohocken, PA*

ASTM:D4254-16 (2016). Standard Test Methods for Minimum Index Density and Unit Weight of Soils and Calculation of Relative Density, *ASTM International, West Conshohocken, PA*

Bauer, R., Leung, W. and Barfoot, T. (2005). Experimental and simulation results of wheel-soil interaction for planetary rovers, *In: Proceedings of IEEE/ RSJ International*

Conference on Intelligent Robots and Systems, Edmonton, Alberta, Canada, IEEE, pp. 586–591.

Bienen, B., Byrne, B., Houlsby, G. and Cassidy, M. (2006). Investigating six-degree-of-freedom loading of shallow foundations on sand, *Géotechnique* **56**(6): 367–380.

Butterfield, R. and Ticof, J. (1979). The use of physical models in design: Discussion, *In Proceedings 7th ECSMFE, Brighton* **4**: 259–261.

Byrne, B. W. and Houlsby, G. T. (2004). Experimental investigations of the response of suction caissons to transient combined loading, *Journal of Geotechnical and Geoenvironmental Engineering* **130**(3): 240–253.

Calvetti, F., Di Prisco, C. and Nova, R. (2004). Experimental and numerical analysis of soil–pipe interaction, *Journal of geotechnical and geoenvironmental engineering* **130**(12): 1292–1299.

Cassidy, M., Byrne, B. and Houlsby, G. (2002). Modelling the behaviour of circular footings under combined loading on loose carbonate sand, *Géotechnique* **52**(10).

Ding, L., Deng, Z., Gao, H., Nagatani, K. and Yoshida, K. (2011). Planetary rovers' wheel—soil interaction mechanics: new challenges and applications for wheeled mobile robots, *Intelligent Service Robotics* **4**(1): 17–38.

Ding, Y., Gravish, N. and Goldman, D. I. (2011). Drag induced lift in granular media, *Physical Review Letters* **106**(2): 028001.

Dou, H. and Byrne, P. M. (1996). Dynamic response of single piles and soil pile interaction, *Canadian Geotechnical Journal* **33**(1): 80–96.

Georgiadis, K. (2010). The influence of load inclination on the undrained bearing capacity of strip footings on slopes, *Computers and Geotechnics* **37**(3): 311–322.

Goldman, D. I. (2014). Colloquium: Biophysical principles of undulatory self-propulsion in granular media, *Reviews of Modern Physics* **86**(3): 943.

Gottardi, G. and Butterfield, R. (1993). On the bearing capacity of surface footings on sand under general planar loads, *Soils and Foundations* **33**(3): 68–79.

Govoni, L., Gourvenec, S. and Gottardi, G. (2010). Centrifuge modelling of circular shallow foundations on sand, *International Journal of Physical Modelling in Geotechnics* **10**(2): 35–46.

Gravish, N., Umbanhowar, P. B. and Goldman, D. I. (2010). Force and flow transition in plowed granular media, *Physical review letters* **105**(12): 128301.

Gravish, N., Umbanhowar, P. B. and Goldman, D. I. (2014). Force and flow at the onset of drag in plowed granular media, *Physical Review E* **89**(4): 042202.

Hambleton, J. P., Stanier, S., White, D. J. and Sloan, S. W. (2014). Modelling ploughing and cutting processes in soils, *Australian Geomechanics* **49**(4): 147–156.

Hansen, J. B. (1970). A revised and extended formula for bearing capacity,*Danish Geotech. Institute Bull.* **98**: 5–11.

Hettler, A. (2010). Possibilities and limitations of 1-g model techniques, *7th International Conference on Physical Modelling in Geotechnics*, Vol. 1, pp. 135–140.

Hong, W. (2001). *Modeling, estimation, and control of robot-soil interactions*, PhD thesis, MIT.

Houlsby, G. and Cassidy, M. (2002). A plasticity model for the behaviour of footings on sand under combined loading, *Géotechnique* **52**(2): 117–129.

Jin, Z., Tang, J., Umbanhowar, P. B. and Hambleton, J. (2019). Preparation of sand beds using fluidization, *engrXiv preprint*: https://doi.org/10.31224/osf.io/u78t9.

Jude, L., David, A. and Ying, C. (2002). Innovative design features of a soil bin to facilitate research on soil-tool interaction, *ASAE Annual International Meeting/CIGR XVth World Congress. July*, pp. 28–31.

Kashizadeh, E., Hambleton, J. and Stanier, S. (2015). A numerical approach for modelling the ploughing process in sands, *In Proceedings of the 14th International Conference of International Association for Computer Methods and Advances in Geomechanics*, Kyoto, Japan, pp. 159–164.

Khot, L. R., Salokhe, V. M., Jayasuriya, H. and Nakashima, H. (2007). Experimental validation of distinct element simulation for dynamic wheel–soil interaction, *Journal of Terramechanics* **44**(6): 429–437.

Kimura, T., Kusakabe, O. and Saitoh, K. (1985). Geotechnical model tests of bearing capacity problems in a centrifuge, *Géotechnique* **35**(1): 33–45.

Kobayakawa, M., Miyai, S., Tsuji, T. and Tanaka, T. (2018). Local dilation and compaction of granular materials induced by plate drag, *Physical Review E* **98**(5): 052907.

Kobayakawa, M., Miyai, S., Tsuji, T. and Tanaka, T. (2019). Interaction between dry granular materials and an inclined plate(comparison between large-scale DEM simulation and three-dimensional wedge model), *Journal of Terramechanics* **90**: 3–10.

Koren, Y. (1985). *Robotics for engineers*, Vol. 168, McGraw-Hill New York et al.

Lauder, K. and Brown, M. (2014). Scaling effects in the 1 g modelling of offshore pipeline ploughs, *8th International Conference on Physical Modelling in Geotechnics* **1**: 377–383.

Leblanc, C., Byrne, B. and Houlsby, G. (2010). Response of stiff piles to random two-way lateral loading, *Géotechnique* **60**(9): 715–721.

Lehane, B. and Liu, Q. (2013). Measurement of shearing characteristics of granular materials at low stress levels in a shear box, *Geotechnical and Geological Engineering* **31**(1): 329–336.

Li, C., Hsieh, S. T. and Goldman, D. I. (2012). Multi-functional foot use during running in the zebra-tailed lizard (callisaurus draconoides), *Journal of Experimental Biology* pp. jeb–061937.

Li, C., Umbanhowar, P. B., Komsuoglu, H., Koditschek, D. E. and Goldman, D. I. (2009). Sensitive dependence of the motion of a legged robot on granular media, *Proceedings of the National Academy of Sciences* **106**(9): 3029–3034.

Li, C., Zhang, T. and Goldman, D. I. (2013). A terradynamics of legged locomotion on granular media, *Science* **339**(6126): 1408–1412.

Loukidis, D., Chakraborty, T. and Salgado, R. (2008). Bearing capacity of strip footings on purely frictional soil under eccentric and inclined loads, *Canadian Geotechnical Journal* **45**(6): 768–787.

Lynch, D. J., Lynch, K. M. and Umbanhowar, P. B. (2020). The soft-landing problem: Minimizing energy loss by a legged robot impacting yielding terrain, *IEEE Robotics and Automation Letters* **5**(2): 3658–3665.

Maciejewski, J. and Jarzebowski, A. (2002). Laboratory optimization of the soil digging process, *Journal of Terramechanics* **39**(3): 161–179.

Maillot, B. (2013). A sedimentation device to produce uniform sand packs, *Tectonophysics* **593**: 85–94.

Maladen, R. D., Ding, Y., Li, C. and Goldman, D. I. (2009). Undulatory swimming in sand: subsurface locomotion of the sandfish lizard, *Science* **325**(5938): 314–318.

Martin, C. (2005). Exact bearing capacity calculations using the method of characteristics, *In Proceedings of the 11th International Conference of IACMAG*, Turin, **4**: 441–450.

Moreland, S. J., Skonieczny, K., Wettergreen, D., Creager, C. and Asnani, V. (2011). Soil motion analysis system for examining wheel-soil shearing, *In International Conference of the International Society for Terrain-Vehicle Systems*, pp. 361-377.

Muro, T. (1989). Tractive performance of a bulldozer running on weak ground, *Journal of Terramechanics* **26**(3-4): 249–273.

Murphy, K. A., Dahmen, K. A. and Jaeger, H. M. (2019). Transforming mesoscale granular plasticity through particle shape, *Physical Review X* **9**(1): 011014.

Murray, R. M. (2017). *A Mathematical Introduction to Robotic Manipulation*, CRC press.

Nasr, A. M. (2013). Experimental and theoretical studies of laterally loaded finned piles in sand, *Canadian Geotechnical Journal* **51**(4): 381–393.

Negro, P., Paolucci, R., Pedretti, S. and Faccioli, E. (2000). Large-scale soil-structure interaction experiments on sand under cyclic loading, *In Proceedings of the 12th World Conference on Earthquake Engineering*, Auckland, New Zealand, p. 1191.

Nezami, E. G., Hashash, Y., Zhao, D. and Ghaboussi, J. (2007). Simulation of front end loader bucket–soil interaction using discrete element method, *International Journal for Numerical and Analytical Methods in Geomechanics* **31**(9): 1147–1162.

O'Loughlin, C. D., Cocjin, M. L., Gourvenec, S. M. and Stanier, S. A. (2018). A simple approach to multi-degree-of-freedom loading in a geotechnical centrifuge, *Geotechnical Testing Journal* **42**(5): 1150–1168.

Qian, F. and Goldman, D. I. (2015). The dynamics of legged locomotion in heterogeneous terrain: universality in scattering and sensitivity to initial conditions., *Robotics: Science and Systems*, pp. 1–9.

Qian, F., Zhang, T., Korff, W., Umbanhowar, P. B., Full, R. J. and Goldman, D. I. (2015). Principles of appendage design in robots and animals determining terradynamic performance on flowable ground, *Bioinspiration and Biomimetics* **10**(5): 056014.

Ricceri, G. and Simonini, P. (1989). Interaction diagrams for shallow footings on sand, *Proceedings of the 12th International Conference on Soil Mechanics and Foundation Engineering*, Rio de Janeiro, pp. 13–18.

Robinson, S., Brown, M. J., Matsui, H., Brennan, A., Augarde, C., Coombs, W. and Cortis, M. (2019). Centrifuge testing to verify scaling of offshore pipeline ploughs, *International Journal of Physical Modelling in Geotechnics* **19**(6): 305–317.

Selig, E. T. and Nelson, R. (1964). Observations of soil cutting with blades, *Journal of Terramechanics* **1**(3): 32–53.

Slonaker, J., Motley, D. C., Zhang, Q., Townsend, S., Senatore, C., Iagnemma, K. and Kamrin, K. (2017). General scaling relations for locomotion in granular media, *Physical Review E* **95**(5): 052901.

Stanier, S. and White, D. (2013). Improved image-based deformation measurement in the centrifuge environment, *Geotechnical Testing Journal* **36**(6): 915–928.

Todorovska, M. I. (2002). Full-scale experimental studies of soil-structure interaction, *ISET Journal of Earthquake Technology* **39**(3): 139–165.

Vahed, S., Song, X., Dai, J., Lam, H., Seneviratne, L. and Althoefer, K. (2008). Soil estimation based on dissipation energy during autonomous excavation, *IFAC Proceedings Volumes* **41**(2): 13821–13826.

Vesic, A. B. (1963). Bearing capacity of deep foundations in sand, *Canadian Highway Research Record*, Report 39.

Vesic, A. S. (1975). Bearing capacity of shallow foundations, *Foundation Engineering Handbook*. pp. 121–147. New York: Van Nostrand Reinhold.

White, D., Take, W. and Bolton, M. (2003). Soil deformation measurement using particle image velocimetry (piv) and photogrammetry, *Geotechnique* **53**(7): 619–631.

Wong, J. (2012). Predicting the performances of rigid rover wheels on extraterrestrial surfaces based on test results obtained on earth, *Journal of Terramechanics* **49**(1): 49–61.

Wong, J. (2014). Terramechanics and its applications to the evaluation of terrestrial and extraterrestrial vehicle mobility: theory into practice, *International Journal of Vehicle Design* **65**(4): 384–410.

Wong, J.-Y. and Reece, A. (1967). Prediction of rigid wheel performance based on the analysis of soil-wheel stresses part i. performance of driven rigid wheels, *Journal of Terramechanics* **4**(1): 81–98.

Wood, D. M. (2014). *Geotechnical modelling*, CRC Press.

Wu, S., Hu, J. and Wong, J. (1984). Behaviour of soil under a lugged wheel, *In Proceedings of 8th ISTVS International Conference*, Cambridge, U.K., pp. 545-559.

Yong, R. and Hanna, A. (1977). Finite element analysis of plane soil cutting, *Journal of Terramechanics* **14**(3): 103–125.